Ninth International Conference on CFD in the Minerals and Process Industries
CSIRO, Melbourne, Australia
10-12 December 2012

MODELLING BUBBLE FLOW WITH CFX AND FLUENT FOR ALUMINIUM REDUCTION CELLS

Peter J. WITT[1*], Yuqing FENG[1], Ingo EICK[2] and M. Phil SCHWARZ[1]

[1] CSIRO Mathematics, Informatics and Statistics, Clayton, Victoria 3169, AUSTRALIA
[2] Hydro Aluminium AS, Neuss, GERMANY
*Corresponding author, E-mail address: Peter.Witt@csiro.au

ABSTRACT

A CFD model of bath flow and alumina transport in an Aluminium reduction cell has been developed using ANSYS/Fluent. The model is based on an earlier ANSYS/CFX model that was validated against PIV measurements.

Initial work using a simple bubble rise test case, showed a large discrepancy between the two models. With refinement of the Fluent model, good quantitative agreement was achieved. The Fluent model required a finer mesh and the use of QUICK differencing.

Information derived from the bubble rise test case was implemented into a full three dimensional, 18 anode, aluminium reduction cell bath flow model. A comparison between the CFX and Fluent models indicated good qualitative agreement. Similar bath and bubble flow patterns were predicted by each model. A detailed comparison showed some quantitative differences between the predictions. These differences in the bath flow field gave rise to some quantitative differences in the predicted alumina distribution.

NOMENCLATURE

D	kinematic diffusion coefficient
$\mathbf{M}$	interphase transfer terms
P	pressure
$\mathbf{S_M}$	momentum source terms
$S_{ci}^{(\Phi)}$	alumina reduction rate
S_c	Turbulent Schmidt number
$\mathbf{U}$	velocity
α	phase, d=gas, c=liquid
γ	volume fraction,
ρ	density
ϕ	alumina mass fraction
μ	effective viscosity

INTRODUCTION

Aluminium metal is reduced from alumina in Hall-Héroult reduction cells; this is the main process for producing primary aluminium metal. Operation of aluminium reduction cells relies on a detailed knowledge of electrochemical, electro-magnetic, heat transfer and hydrodynamic processes occurring in the cells.

In the Hall-Héroult process alumina particles are feed on to the top of a bath containing molten cryolite, the alumina then dissolves into the bath. Anodes, partially immersed into the top of the bath, supply an electrical current that drives an electrochemical reaction that reduces alumina to aluminium metal and oxygen. The evolved oxygen reacts with the carbon anodes to form carbon dioxide and the aluminium accumulates as a layer of molten metal in the bottom of the cell. Carbon dioxide gas forms bubbles under the anode while buoyancy forces cause these bubbles to travel along the anode's base, before they rise to the surface beside the anode. A strong internal flow of the liquid bath is established by the bubble motion and this acts to transport alumina and heat through the bath.

Aluminium reduction cells operate in a harsh environment as the bath is molten cryolite, known to dissolve most engineering materials, and at a temperature of approximately 970°C. Electrical currents in the range of 100 to 450 kA are typical in reduction cells. Such currents induce strong magnetic fields, which act on conducting liquids and the bath, inducing secondary flows by Lorentz forces. These conditions along with restricted access make measurements on operating cells very difficult and greatly limit the amount of information that can be obtained from operating cells.

To develop new cells and to improve the economic and environmental performance of existing cells, new tools are needed. Mathematical models provide a tool to understand and explore how changes to cell geometry and operation affect performance (Gusberti *et al.* 2012). For example, Moxnes *et al.* (2009) described how optimised alumina feeding through experimentation can improve performance. However, experimentation is very costly and time consuming. Validated mathematical models can provide a more efficient means of achieving improved cell performance.

It is usual practice to use air-water models to understand bubble drive bath flow in aluminium reduction cells (Solheim *et al.*, 1989 and Purdie *et al.* 1993). As an alternative to physical experimentation, CSIRO has developed (Feng *et al.* 2006) and validated (Feng *et al.* 2010b) a two phase CFD model of the bath flow. An extension of the model has been developed to include alumina feeding, transport and reduction. This model allows alumina distribution within the cell and feeding policies to be investigated; such an investigation was reported by Feng *et al.* (2010a).

Previous work at CSIRO has been performed using ANSYS/CFX (ANSYS, 2009) as the numerical solver. More recently we have replicated the model in ANSYS/Fluent (ANSYS, 2010) to allow easy interchange of

results from other models. In the process a comparison between the two codes was used to validate the Fluent implementation of the bath flow and alumina mixing models. This paper reports on the implementation and information obtained from the process.

MODEL DESCRIPTION

Bath Flow Model

Flow of gas and liquid in the bath is modelled using a steady-state two phase Eulerian-Eulerian model where transport equations given below are solved for phase volume fraction and velocity.

$$\nabla \bullet (\gamma_\alpha \rho_\alpha \mathbf{U}_\alpha) = 0 \tag{1}$$

$$\nabla \bullet (\gamma_\alpha (\rho_\alpha \mathbf{U}_\alpha \otimes \mathbf{U}_\alpha)) = -\gamma_\alpha \nabla P_\alpha + \nabla \bullet (\gamma_\alpha \mu_\alpha (\nabla \mathbf{U}_\alpha + (\nabla \mathbf{U}_\alpha)^T)) + \mathbf{S}_{M\alpha} + \mathbf{M}_\alpha \tag{2}$$

Additional source terms, $\mathbf{S}_{M\alpha}$, are needed to account for buoyancy and the Lorentz force. Inter-phase terms, $\mathbf{M}_\alpha$, are added for inter-phase drag, which is based on the Ishii and Zuber (1979) model, and for turbulent dispersion based on the model of Lopez de Bertodano (1991). Bubble diameter varies within the domain and is based on experimental observations.

Turbulent effects in the liquid phase are account for by an extension of the two equation k-ε model. Gas phase turbulent viscosity is obtained from the liquid phase values based on a zero equation approach. Additional source terms are added to the k and ε equations to account for bubble induced turbulence.

For brevity details of the various models are not included here but interested readers are referred to Feng, *et al.* (2010b) for further details of the model and its validation against PIV measurements.

Alumina Mixing Model

Once a steady-state bath flow is calculated from the Bath Flow Model a transient simulation of alumina within the liquid phase is performed by solving a transport equation for the alumina mass fraction.

$$\frac{\partial}{\partial t}(\gamma_c \rho_c \phi_{ci}) + \nabla \bullet (\gamma_c \rho_c \mathbf{U}_c \phi_{ci}) - \nabla \bullet (\gamma_c (\rho_c D_{ci}^{(\phi)} + \frac{\mu_{tc}}{Sc_{tc}}) \nabla \phi_{ci}) = S_{ci}^{(\Phi)} \tag{3}$$

A source term for alumina consumption is added, $S_{ci}^{(\Phi)}$, under the anodes to account for reduction of alumina. Further details of the alumina mixing model are reported in Feng *et al.* (2011).

BUBBLE RISE TEST CASE

Description

A simple test case has been used to assist in the implementation and testing of the model in Fluent. The case is a vertical column filled with liquid and has a central jet through which air enters at a velocity of 0.01 m s^{-1} and gas leaves the top through a degassing boundary. At the sides and base, walls are used. The system is essentially two-dimensional; however four cells are included in the third direction with symmetry planes applied in the depth direction. The use of three dimensions is to assist with code development as the full cell model is by necessity three dimensional. Two different meshes have been used and these are shown in Figure 1. Mesh 1 is a uniform mesh, Mesh 4 has the same vertical spacing but is refined at the centre and near the side walls.

(a) Mesh 1 (b) Mesh 4

Figure 1: Meshes used for bubble rise test case

Results

The plot on the left in Figure 2 shows the gas distribution for the CFX model without the additional source terms for turbulent dispersion and bubble induced turbulence. Results in the centre and on the right are for CFX and Fluent models with the additional source terms included. The effect of these additional terms on laterally dispersing the bubble plume is very marked.

Influence of the mesh resolution on liquid velocity, gas distribution and turbulent production for CFX was assessed. Results are shown in Figure 3 as a series of plots along the three green horizontal lines shown in Figure 1. The lines are 0.05, 0.1 and 0.15 m above the base on the geometry. Only a small difference in the results is observed between the two meshes. These results were obtained using the "High Resolution" scheme for convective terms in the equations, which is a bounded and essentially second order differencing scheme.

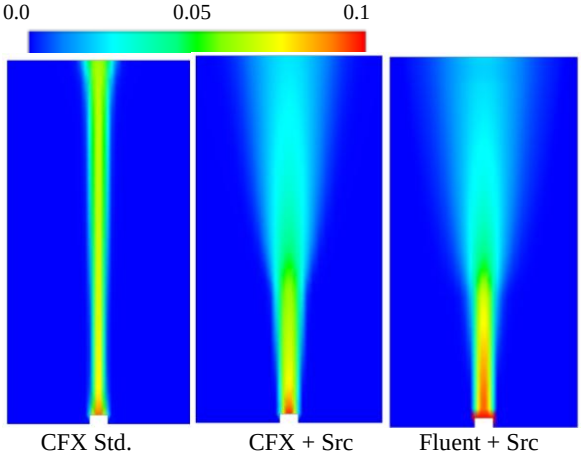

Figure 2: Plots of gas volume fraction for Mesh 4.

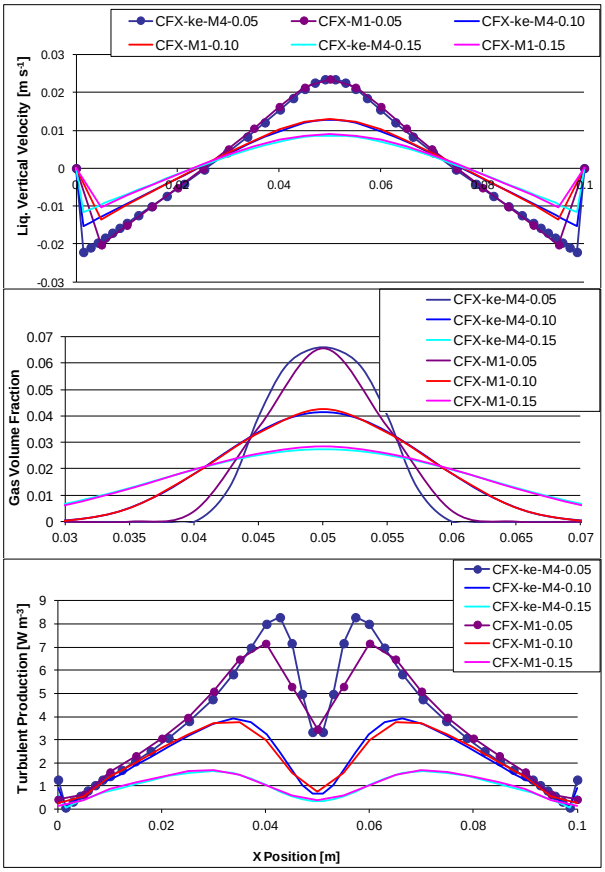

Figure 3: Plots of liquid vertical velocity (top), gas volume fraction (centre) and turbulent production (bottom) at 3 locations for CFX on the two meshes (M1 = Mesh 1 & M4 = Mesh 4, 0.05, 0.1 and 0.15 are the distance above the inlet).

A similar comparison of predicted flow profiles using the two meshes and Fluent as the solver are plotted in Figure 4. The liquid velocity profile shows that refining the mesh significantly alters the velocity profile both in the central plume and near the walls. On the coarse mesh, Mesh 1, the results were not sensitive to the differencing scheme. On the fine mesh results were sensitive to the differencing scheme with the results shown obtained using QUICK. One of the reasons for such a difference in the velocity profiles between the meshes appears to be the turbulence production. The coarse mesh model has very large turbulence production near the walls but much lower values in the bubble plume when compared to both the fine mesh Fluent and the CFX results in Figure 3.

Results for CFX and Fluent using the fine mesh are compared in Figure 5 indicating that good agreement is achieved between the two codes. To achieve this agreement in the Fluent model it was necessary to use QUICK differencing for the convection terms. Wall boundary conditions in the CFX model used "Scalable Wall Functions". This boundary condition was trialled in Fluent but it did not give significantly different results to the standard logarithmic turbulent wall functions. To match the CFX results the "Enhanced Wall Function" model in Fluent was used.

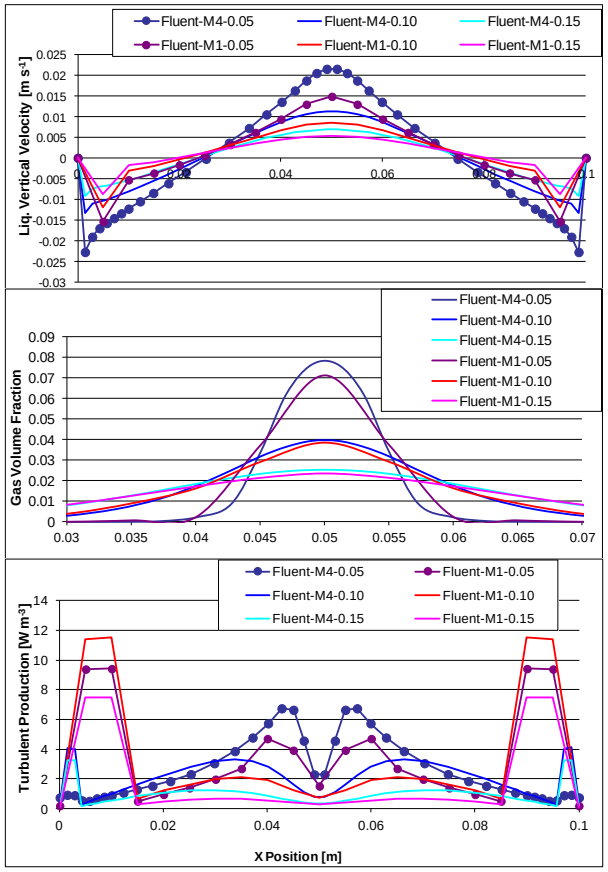

Figure 4: Plots of liquid vertical velocity (top), gas volume fraction (centre) and turbulent production (bottom) at 3 locations for Fluent on the two meshes.

Results from these tests indicate that the CFX Bath Flow model physics has been successfully implemented into Fluent. For a simple test case Fluent was found to give similar results to CFX but requires a finer mesh near walls and regions of step gradients.

FULL CELL MODEL

Description

Having demonstrated that the key model physics had been successfully implemented into Fluent, a full 3D model of a reduction cell was modelled in Fluent. The full cell model is 6.42 m long, 3.32 m wide and the bath depth is 200 mm, it has 18 anodes of length 1.3 m and width 0.65 m with an anode to cathode distance (ACD) of 40 mm. Figure 6 shows a view of the model geometry. Further details of the full cell model geometry and flow conditions are described by Feng *et al.* (2010b). The ANSYS/Workbench mesher was used to generate a hexahedral mesh consisting of approximately 270,000 hexahedral cells, the mesh is larger than the previously reported CFX mesh. This was because preliminary simulations and the bubble rise test case indicated that it was necessary to increase the number of cells across the side and end channels.

Boundary conditions for the model consist of:

- Gas generated at the base of each anode, which is implemented with source terms, enters the model at a rate of 0.0157 kg s^{-1},
- A degassing boundary at the top surface of the model, with liquid bath treated as a free-slip wall and gas is able

to leave the model; this was developed by the authors and tested in the bubble rise test case,

- The remaining surfaces are considered walls with a no-slip condition for the liquid and free-slip for the gas.

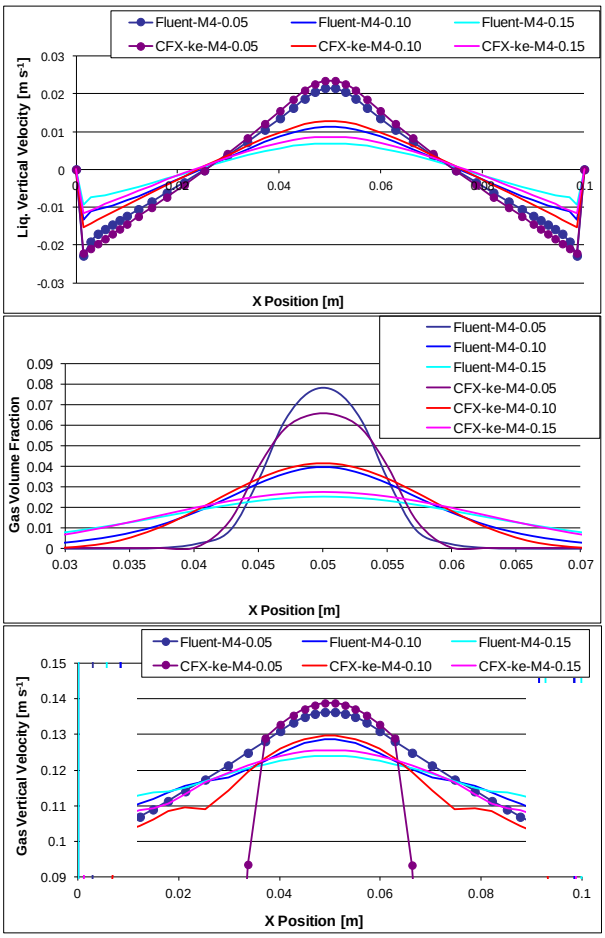

Figure 5: Plots of liquid vertical velocity (top), gas volume fraction (centre) and gas vertical velocity (bottom) at 3 locations for Fluent and CFX on Mesh 4.

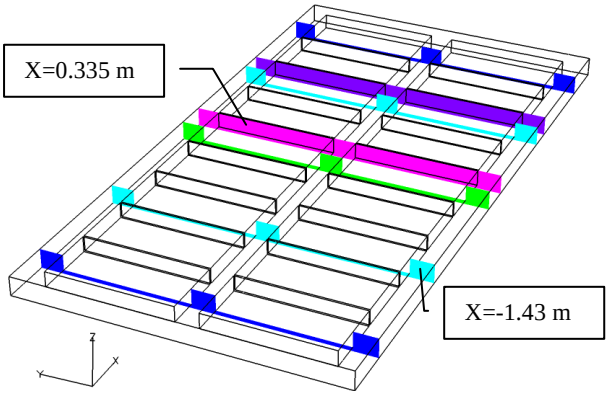

Figure 6: Geometry of the 18 anode full cell model.

Bath Flow Results

Results for the steady state full cell model have been obtained for both the CFX and Fluent models using the same geometry, mesh and flow rates. Streamlines of liquid bath flow that originate under the anodes are plotted in Figure 7 and show strong recirculation in the side and end channels. For the 14 anodes not adjacent to the end channels the streamlines show flow into the ACD from the side and centre channels and out from the ACD into the inter-anode gaps. As evident from the streamlines, liquid flow under the four anodes near the end channels is predominantly from the end channel and along the cell to the inter-anode gap, with some flow also to the side and centre channels. Both models predict similar bath flow behaviour with slightly higher velocities predicted by the Fluent model in the channels.

Detailed plots of the liquid bath velocity through the centre of an anode at X=-1.43 m is shown in Figure 8 and along the centre of an inter-anode gap at X=0.335 m is shown in Figure 9. Location of the planes is indicated in Figure 6. As bath flow is predominantly symmetric about the centre channel only one side of the cell is shown. Both models predict strong recirculation in the side channel and a pair of counter rotating cells in the centre channel. In the centre channel gas bubbles drive the liquid flow up the end of the anodes, across the free surface and down at the centre of the channel. CFX results have this down flow located at the middle of the centre channel. Results from the Fluent model predict that the down flow location varies along the cell due to the predicted flow not being completely stable. Fluent also predicts slightly higher velocities than the CFX model. Behaviour in the side channels is similar with bubbles rising next to the anode and downward flow near the cell wall.

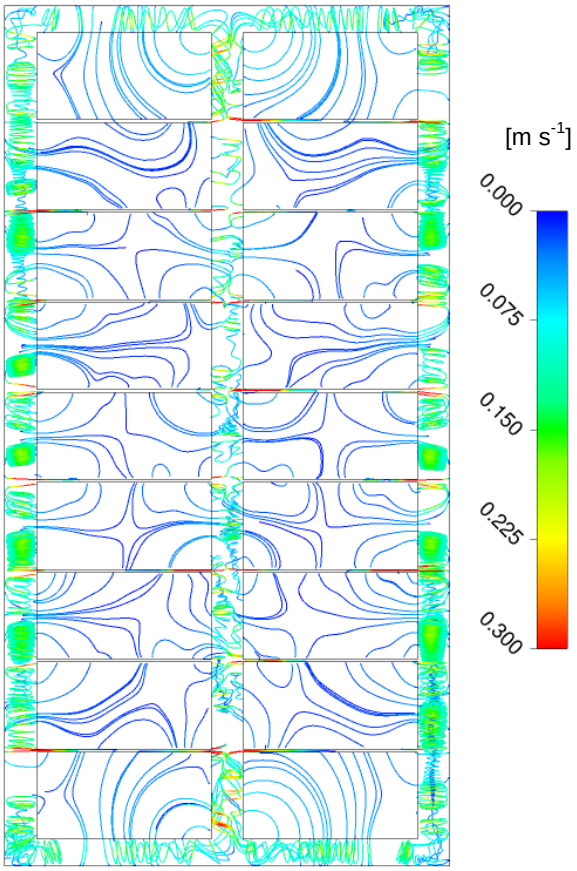

Figure 7: Streamlines of bath velocity originating from under the anodes predicted by the Fluent model.

A substantial amount of gas is released from under the anode, via the inter-anode gap. This is shown in Figure 10 by high gas volume fractions plotted on a vertical plane in the inter-anode gap at X=0.335 m. Velocity vectors for the CO_2 gas are plotted in the inter-anode gap in Figure 11.

Both models show good agreement for the flow in these gaps with the flow pattern and magnitude being similar. Gas bubble distribution and gas velocities predicted by each model are generally in good agreement.

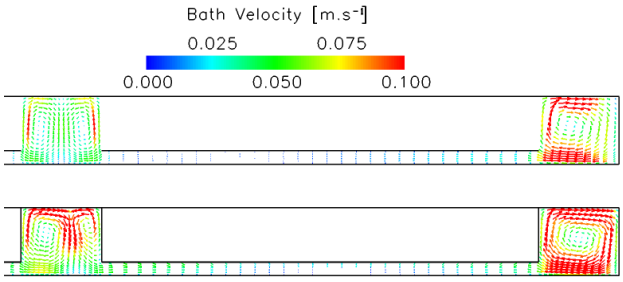

Figure 8: Liquid bath velocity vectors on a plane through the anode centre at x=-1.43, CFX (top) Fluent (bottom).

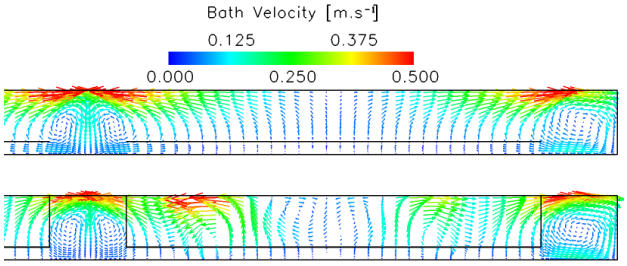

Figure 9: Liquid bath velocity vectors in the inter-anode gap at x=0.335, CFX (top) Fluent (bottom).

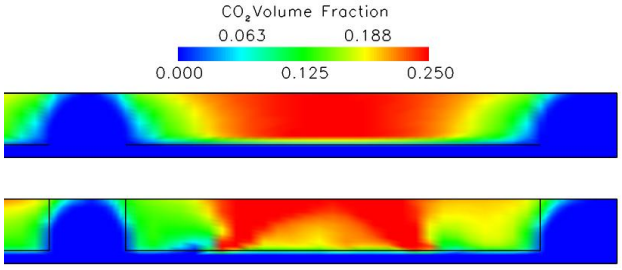

Figure 10: CO_2 gas volume fraction in the inter-anode gap at x=0.335, CFX (top) Fluent (bottom).

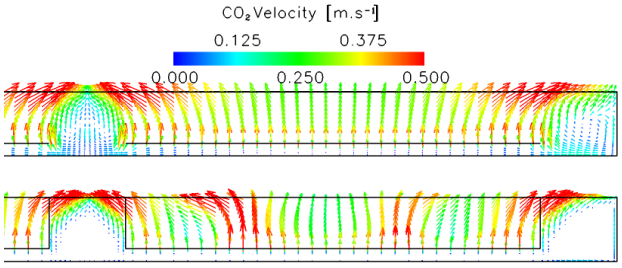

Figure 11: CO_2 gas velocity vectors in the inter-anode gap at x=0.335, CFX (top) Fluent (bottom).

Alumina Mixing Results

A transient simulation of alumina mixing and consumption was run in both CFX and Fluent using the gas and liquid flow fields from the steady state models presented in the previous section. Initially a uniform alumina concentration of 0.035 was assumed, with alumina feed to the cell at four locations along the centre channel. Alumina feeding locations are shown in Figure 12, with details of the feeding cycle and the consumption model given in Feng *et al.* (2010a).

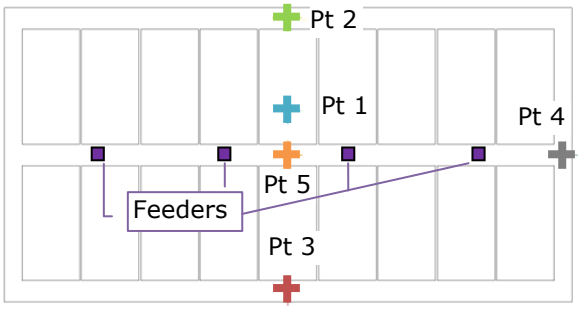

Figure 12: Location of alumina sampling points and feeders.

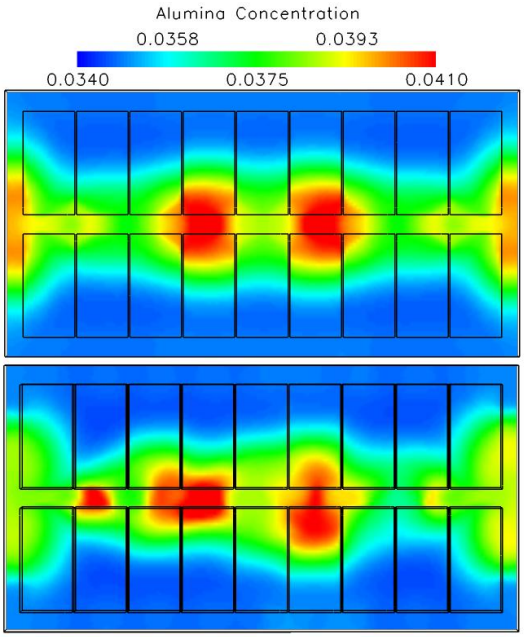

Figure 13: Alumina mass fraction at a time of 60 sec. on a plane through the centre of the ACD, CFX (top) Fluent (bottom).

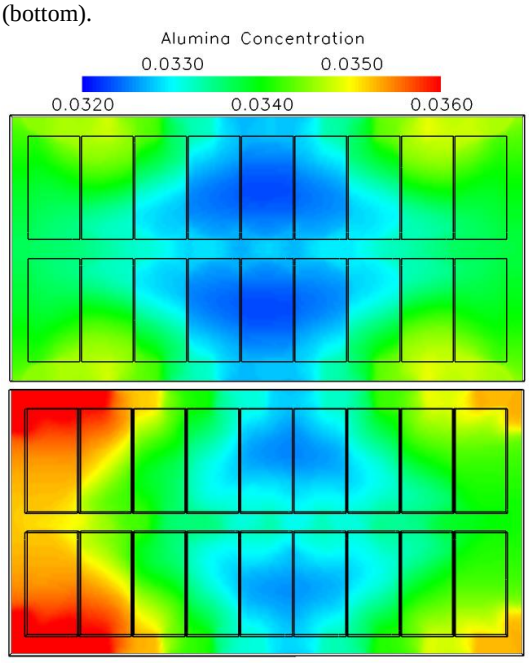

Figure 14: Alumina mass fraction at a time of 2940 sec. on a plane through the centre of the ACD, CFX (top) Fluent (bottom).

Strong vertical velocities in the cell produce strong mixing in the vertical direction. There is thus very little vertical variation in the alumina concentration relative to the lateral variation. For this reason vertical plots of alumina concentration are not presented here.

After 1 minute, results in Figure 13 show that alumina has dispersed under the anodes from the two feeder locations near the centre of the cell and into the end channels from the two outer feeders. In the CFX results the alumina is dispersed very symmetrically into a quarter symmetry pattern. Whilst the Fluent results also exhibit the quarter symmetry pattern, they have variations end-to-end and side-to-side. This variation is likely to be a result of the predicted bath flow in the Fluent model. Results in Figure 14, at the end of the feeding cycle, show that after a significant time without feeding regions of relatively low alumina concentration occurs under the centre anodes.

Transient alumina concentration is monitored at five point locations shown in Figure 12. The change in alumina concentration with time at each of these sampling locations is plotted in Figure 15 and shows that there is large variations in the alumina concentration with time and location in the cell. These plots show excellent agreement between the CFX and Fluent models. Results for Point 1, which is in the ACD near the centre of the cell, shows some differences during the overfeeding period of 1400 to 1900 seconds. This difference is most likely due to the slightly different flow behaviour predicted in the centre channel by the Fluent model.

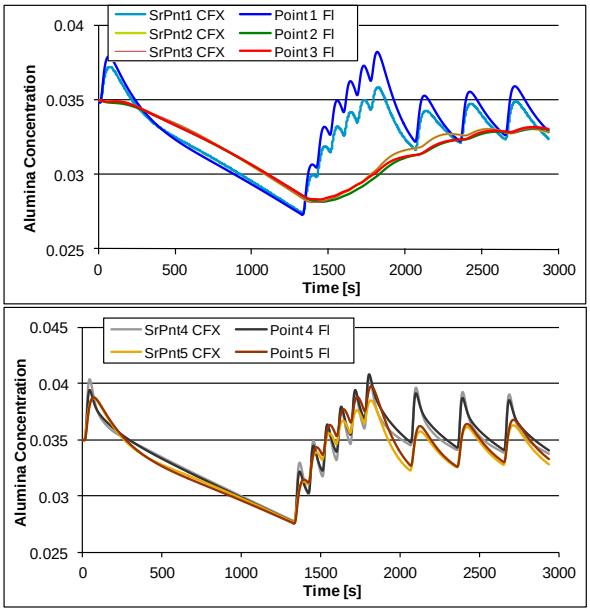

Figure 15: Variation in alumina concentration, with time, at various locations in the bath. Locations of the sampling points are shown in Figure 12.

CONCLUSION

A previously published aluminium cell bath flow model has been transferred to Fluent. Key physics including gas-liquid inter-phase momentum transfer, bubble induced turbulence, turbulent dispersion force and alumina dispersion and consumption models have been implemented into Fluent.

Testing of the model for a bubble rise case shows good qualitative agreement. Reasonable quantitative agreement was achieved but required a finer mesh and the use of QUICK differencing in the Fluent model. Furthermore the CFX model showed little sensitivity to the mesh resolution while the Fluent model showed significant sensitivity to the mesh and numerical scheme used.

A three dimensional, 18 anode, model of the bath of a full reduction cell was setup in Fluent and run to obtain steady-state bath and bubble flow fields. These flows were then used to predict transient alumina transport, mixing and consumption in the cell. Flow results from the Fluent model were compared to those obtained from a previously validated CFX model. Qualitatively the two models predict similar bath and bubble flow patterns. Detailed comparisons show some difference in the quantitative values predicted by the models, with slightly higher velocities predicted by Fluent. Comparison of the transient alumina distribution predicted by the two models shows that they are in excellent agreement.

A complex multiphase model of bubble and MHD driven flow, based on a published CFD model, has been incorporated into Fluent. Differences in the underlying numerical methods of the two solvers mean that finer meshes are required in the Fluent model to match the CFX results.

REFERENCES

ANSYS, (2009), *ANSYS/CFX Release 12 User Manual*, ANSYS Inc.

ANSYS, (2010), *ANSYS/Fluent Release 13 User Manual*, ANSYS Inc.

GUSBERTI, V., SEVERO, D.S., WELCH, B.J., & SKYLLAS-KAZACOS, M., (2012), "Modeling the mass and energy balance of different aluminium smelting cell technologies", *Light Metals 2012*, 929-934.

FENG, Y.Q., YANG, W., COOKSEY, M. & SCHWARZ, M.P., (2006), "CFD model of bubble driven flow in aluminium reduction cells and validation using PIV measurement", *5th Int. Conf. on CFD in the Process Industries*, Melbourne, Australia.

FENG, Y.Q., COOKSEY, M. & SCHWARZ, M.P. (2010a), "CFD Modelling of Alumina Mixing in Aluminium Reduction Cells", *Light Metals 2010*, 455-460.

FENG, Y.Q., YANG, W., COOKSEY, M. & SCHWARZ, M.P., (2010b), "Development of Bubble Driven Flow CFD Model Applied for Aluminium Smelting Cells", *J. Comp. Multiphase Flows*, **2(3)**, 179-188.

FENG, Y.Q., COOKSEY, M. & SCHWARZ, M.P., (2011), "CFD Modelling of alumina mixing in aluminium reduction cells", *Light Metals 2011*, 543-548.

ISHII, M. and ZUBER, N., (1979), "Drag coefficient and relative velocity in bubbly, droplet or particulate flows", *AIChE J.*, **25**, 843-855.

LOPEZ DE BERTODANO, M., (1991), *Turbulent bubbly flow in a triangular duct*, Ph.D. Thesis, Rensselaer Polytechnic Institute, New York.

MOXNES, B., SOLHEIM, A., LIANE, M., SVINSÅS, E. And HALKJELSVIK, A., (2009), "Improved cell operation

by redistribution of the alumina feeding", *Light Metals 2009*, 461-466.

PURDIE, J.M.. BILEK, M., TAYLOR, M.P., ZHANG, W.D., WELCH, B.J. AND CHEN, J.J.J, (1993), "Impact of anode gas evolution on electrolyte flow and mixing in aluminium electrowinning cells", *Light Metals*, 355-360.

SOLHEIM, A., JOHANSEN, S.T., ROLSETH, S. & THONSTAD, J., (1989), "Gas induced bath circulation in aluminium reduction cells", *Journal of Applied Electrochemistry*, **19**, 703-712.

ACKNOWLEDGEMENT

The authors wish to thank Hydro Aluminium AS for providing financial and other support that enabled this work to be published.

This work was conducted under the auspices of CSIRO's Minerals Down Under Flagship.

